Article

Performance Analysis of a Synchronous Reluctance Generator with a Slitted-Rotor Core for Off-Grid Wind Power Generation

Samuel Adjei-Frimpong and Mbika Muteba *

Department of Electrical and Electronic Engineering Technology, University of Johannesburg, Auckland Park, Johannesburg 2006, South Africa; 221182514@student.uj.ac.za
* Correspondence: mmuteba@uj.ac.za

Abstract: In this paper, the performance of a Dual-Stator Winding Synchronous Reluctance Generator (SynRG) suitability for off-grid wind power generation is analyzed. The rotor of the SynRG has a slitted-rotor core to improve selected vital performance parameters. The SynRG with a slitted-rotor core was modeled using a two-dimensional (2D) Finite Element Method (FEM) to study the electromagnetic performance of key parameters of interest. To validate the FEA results, a prototype of the SynRG with a slitted rotor was tested in the laboratory for no-load operation and load operation for unity, lagging, and leading power factors. To evaluate the capability of the SynRG with a slitted-rotor core to operate in a wind turbine environment, the machine was modeled and simulated in Matlab/Simulink (R2023a) for dynamic responses. The FEA results reveal that the SynRG with a slitted-rotor core, compared with the conventional SynRG with the same ratings and specifications, reduces the torque ripple by 24.51%, 29.72%, and 13.13% when feeding 8 A to a load with unity, lagging, and leading power factors, respectively. The FEA results also show that the induced voltage on no-load of the SynRG with a slitted-rotor core, compared with the conventional SynRG of the same ratings and specifications, increases by 10.77% when the auxiliary winding is fed by a capacitive excitation current of 6 A. Furthermore, the same results show that with a fixed excitation capacitive current of 6 A, the effect of armature reaction of the SynRG with a slitted-rotor core is demagnetizing when operating with load currents having a lagging power factor, and magnetizing when operating with load currents having unity and leading power factors. The same patterns have been observed in the experimental results for different excitation capacitance values. The Matlab/Simulink results show that the SynRG with a slitted-rotor core has a quicker dynamic response than the conventional SynRG. However, a well-designed pitch-control mechanism for the wind turbine is necessary to account for changes in wind speeds.

Keywords: dual-stator winding; dynamic performance; finite element analysis; performance analysis; synchronous reluctance generator; slitted-rotor core; torque ripple; wind turbine application

1. Introduction

In the past decades, there has been a steady increase in the use of renewable power generation, particularly solar and wind power, to help alleviate the world energy crisis, combat climate change, and reduce the dependency on fossil fuels, which are the main source of atmospheric pollution. With the recent increase in wind power generation, mainly due to the installation of large-scale grid-connected wind turbines and the recent load demand increase in urban areas in most parts of the world, self-stand or self-excited micro-wind generating systems (<10 kW) are increasingly becoming a practical option for stable

electricity supply. Urban environments are noise sensitive, and wind turbines used in these environments must be designed to reduce noise pollution, reduce vibration to prevent damage to the structures on which they are installed, and aesthetically blend into the urban landscape without becoming eyesores. A well-designed wind energy system can be integrated with solar panels (already installed on most urban rooftops) for more reliable, year-round urban electrification [1].

The most common electrical machines for a self-excited generating system are the Permanent Magnet Synchronous generator (PMSG), the Brushless Direct Current Machine (BLDCM), and the Self-excited Induction Generator (SEIG). The PMSG has higher efficiency, higher power density, no additional power supply for the magnet field excitation, and higher reliability due to the absence of mechanical components such as carbon brushes and slip rings [2]. However, PMSG designs are based on rare-earth magnetic materials, namely, Neodymium–Boron–Iron (NdFeB) grades, with higher remanence and coercive values. Recently, the increased demand for electric vehicles has led to a sharp increase in demand for rare-earth magnets [3]. The SEIG offers advantages over the traditional Double Fed Induction Generator (DFIG), such as rugged construction, reduced size, absence of a DC source for field excitation, and low maintenance. However, the SEIG is reported to have low efficiency, poor voltage regulation, and is unsuitable for variable-speed applications. In addition, the generated voltage frequency is influenced by the connected load and excitation capacitor [4].

The Synchronous Reluctance Machine (SynRM), in recent years, has emerged as a competitor to the Permanent Magnet (PM) machines and Induction Machines (IMs) for standalone wind power generation due to its robustness, simple rotor construction with no copper losses, high torque density, no magnets (thereby removing the problem of demagnetization), lower rotor inertia, and comparatively lower cost than the Brushless Direct Current Machines (BLDCMs) and the Permanent Magnet Synchronous Machines (PMSMs) [5–8]. Despite the several advantages of the SynRM over the traditional IMs and PMSMs, it is characterized by poor power factors, high torque ripples, and other secondary effects such as rotor iron losses, vibration, and noise [9]. As shown in [10,11] on the design of Synchronous Reluctance Machines (SynRMs), the rotor geometry significantly influences machine torque performance. The torque ripple was affected more significantly by the variation of the flux barrier pitch angle, whilst the average torque was more significantly affected by the variation in the barrier width. Research has been carried out on rotor geometry to improve the torque performance of SynRMs [12–14]. The Synchronous Reluctance Generator (SynRG) analyzed in this article is designed with a slitted-rotor core to have an improved torque and low torque ripple and is more suitable for urban, small power generation when driven by a Vertical Axis Wind Turbine (VAWT). The detailed design of the SynRG with a slitted-rotor core has been reported in [15]. A slit cut-out in the *d*-axis of the rotor is aimed to improve flux distribution, reduce eddy current losses, and further reduce the overall weight of a relatively lighter-weight flux barrier rotor, thereby reducing the inertia of the rotor to enhance its dynamic response [15]. The very low inertia means power generation starts at lower wind speeds, enhancing the overall energy yield in urban environments with inconsistent wind speeds. The VAWTs are better at capturing wind from multiple directions, making them more suited for urban areas where wind patterns are often unpredictable and turbulent due to buildings and other structures [16,17]. The absence of magnets and lower torque ripples also means that the SynRG with a slitted-rotor core coupled to a VAWT reduces vibration and noise pollution, which is particularly important in urban areas.

Self-excitation is initiated and maintained through a capacitor bank connected to the stator's three-phase auxiliary winding, which supplies the necessary reactive power for the generator. Given that the main three-phase winding shares the same magnetic structure,

and it is magnetically coupled to the three-phase auxiliary winding, then, by transformer action, an EMF of similar sinusoidal characteristics is induced in the three-phase main winding. Multi-stator topology self-excited machines started as early as 1930 when Alger and peers reported the use of two identical winding on the stator of an AC generator with the aim of increasing the total power capability of large synchronous generators [18]. Since then, several researchers improved the performance of induction and reluctance machines using dual stator winding with secondary winding connected to a balanced capacitor bank [19–25]. The work reported in [22,23] utilized a set of three-phase auxiliary windings connected to a balanced capacitance to improve the performance characteristics of the SynRM with a simple salient rotor structure. Whilst the work reported in [22,23] was found satisfactory, there is no evidence on experimental measurements to validate the enhancement of torque due to auxiliary capacitive winding. The work reported in [24] employed an auxiliary DC-source-fed single-phase control winding, which was found to improve the power factor but remained silent on the effect of DC-fed auxiliary winding on the machine torque performance. Furthermore, the use of auxiliary capacitive winding was extended to line-start SynRM to improve the performance during transient and steady-state regimes [22,24]. The work in [18] focused on a single-phase SynRM with cage bars mounted on the salient structure of the rotor, while the work in [23] focused on a three-phase SynRM with cage bars inserted in flux barriers of a transverse laminated rotor core. The simulation and experimental results reported in both [22,23] have enhanced torque characteristics during transient and steady-state regimes. This article presents the performance evaluation of a dual stator winding SynRG with a slitted-rotor core, which has yet to be reported for off-grid Vertical Wind Turbine power generation. The organization of this article is as follows: Section 2 presents the materials and methods. Section 3 discusses the Finite Element Analysis (FEA) results. Section 4 reports on the analysis of experimental results, and Section 5 evaluates the dynamic behaviors of the SynRG in a wind turbine environment. Key findings and recommendations are summarized in Section 6.

2. Materials and Methods

2.1. Machine Topology

In this work, the stator of the SynRG is provided with two separate three-phase windings, namely, main and auxiliary. The main winding (u, v, w) is a three-phase single-layer full-pitched winding designed with a DC resistance of 0.7 Ω/phase, and a nominal voltage of 380 V. The auxiliary winding is also a three-phase full-pitched winding (x, y, z), and its coils occupy the top slots near the airgap. The auxiliary winding is designed with a DC resistance of 1.36 Ω/phase. For the SynRM to operate as a standalone generator, the rotor must be rotated by a prime mover (i.e., wind turbine) through a gearbox to ensure that the low-speed wind turbine matches a high-speed SynRG. The stator three-phase auxiliary windings are then fed from a capacitor bank to provide the necessary excitation current to the generator.

Both windings have been designed to provide six magnetic poles when energized. The slitted-rotor core consists of laminations with four flux barriers per pole. The barriers are C-shaped with straight segments. The outer barriers have symmetrical arrangements, but the first three outer barriers from the shaft have different widths to that of the inner barriers. The slit cuts in the *d*-axis of the rotor aimed to improve flux distribution, reduce eddy current losses in the rotor, and reduce the overall weight of the rotor, thereby reducing the inertia of the rotor to enhance its dynamic response. Figure 1 shows the off-grid wind turbine topology and the schematic of SynRG with direct capacitance injection. The direct capacitance injection coupled with a novel slitted rotor ensures improved average torque and minimizes torque ripple.
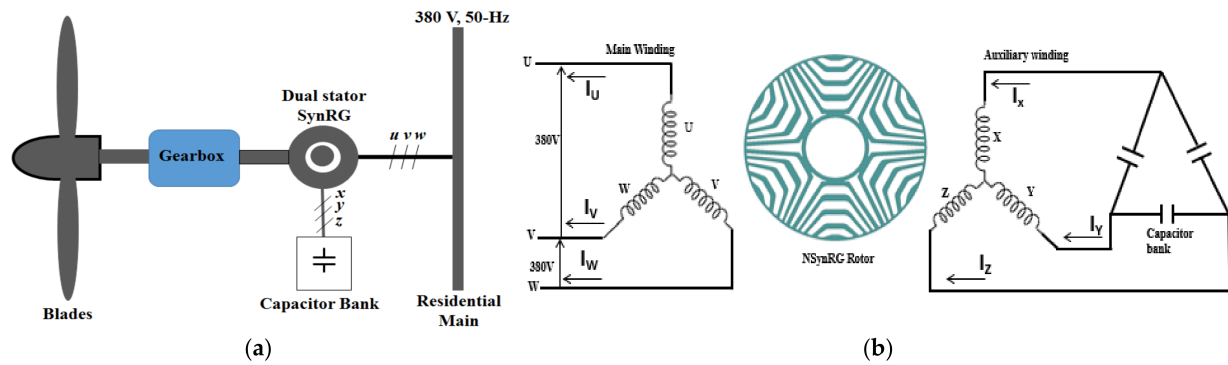
Figure 1. Synchronous Reluctance Generator with direct capacitance injection. (**a**) Off-grid wind turbine topology, (**b**) Schematic diagram of the self-excited NSynRG winding scheme.

2.2. Machine Specifications and Approach

Figure 2a–c show a two-dimensional (2D) cross-section of the slitted-rotor core, conventional rotor core and the stator windings' arrangements, respectively. The ratings and specifications of the SynRG with a slitted-rotor core are given in Table 1. The detailed design and optimization of the SynRM with a slitted-rotor core are reported in [15]. The auxiliary winding coils are shifted from the main winding coil by a slot pitch to mitigate some of the secondary phase-belt harmonics due to the interaction of the magnetomotive forces caused by the currents flowing in the two windings.
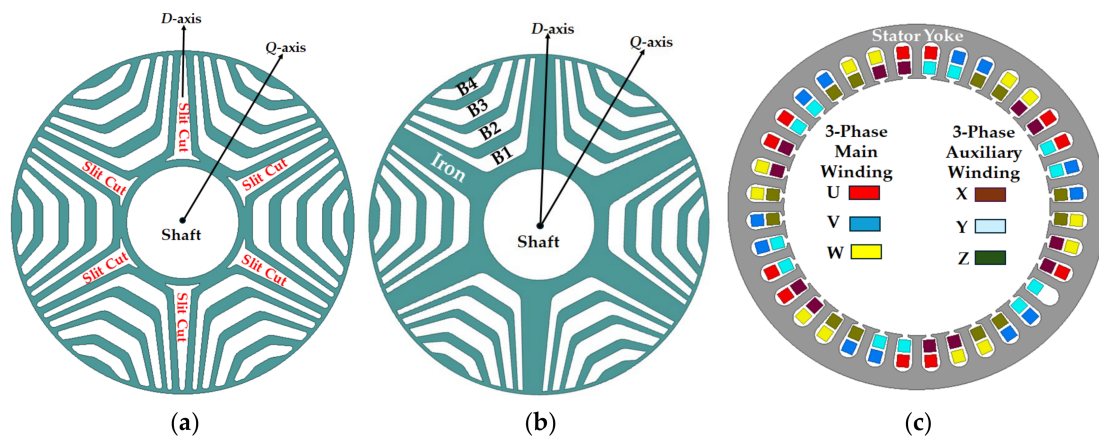

Figure 2. Cross-sections of the rotor of SynRG and stator with two sets of windings. (**a**) Rotor with slit-cuts on *d*-axis, (**b**) Conventional rotor, (**c**) Stator showing the arrangement of both main and auxiliary windings.

The ANSYS Electronic desk package is utilized to perform the numerical analysis of the self-excited SynRG with slitted-rotor core key performance parameters of interests. The MATLAB/Simulink package is used to simulate the dynamic behavior of the SynRG, and the results are compared to those of the conventional SynRG. A prototype of the self-excited SynRG with a slitted-rotor core is tested to validate the FEA results. Figure 3 shows the photographs of the different constituents of the SynRG with a slitted-rotor core, while the photographs of the laboratory setups are shown in Figure 4. The laboratory setup in Figure 4a consists of a three-phase self-excited SynRG with a slitted-rotor core, with its auxiliary winding connected to a delta connected capacitor bank. To monitor and store advanced power data, the Dranetz Power Visa 4400 three-phase power analyzer with eight independent channels is used. The Tektronix TPS 2024 four-channel digital oscilloscope is employed to analyze the output electrical parameters of interest.

Table 1. Machine ratings and specifications.

Ratings/Dimensions/Parameters	Unit	Value
Rated main winding current	A	10
Rated auxiliary current	A	6
Rated Output power	kW	4
Line voltage	V	380
Rated Frequency	Hz	50
Number of poles	-	6
Main windings turn/coil	-	13
Auxiliary windings turn/coil.	-	13
Slot filling factor (Main)	%	36.12
Slot filling facto (Auxiliary)	%	21.67
Total filling factor	%	57.79
Current Density (Main and Aux)	A/mm^2	6.25
Main winding resistance	Ω/phase	0.7
Auxiliary winding resistance	Ω/phase	1.36
Shaft Radius	mm	48
Stack Length	mm	149
Rotor diameter	mm	147

(a) (b) (c)
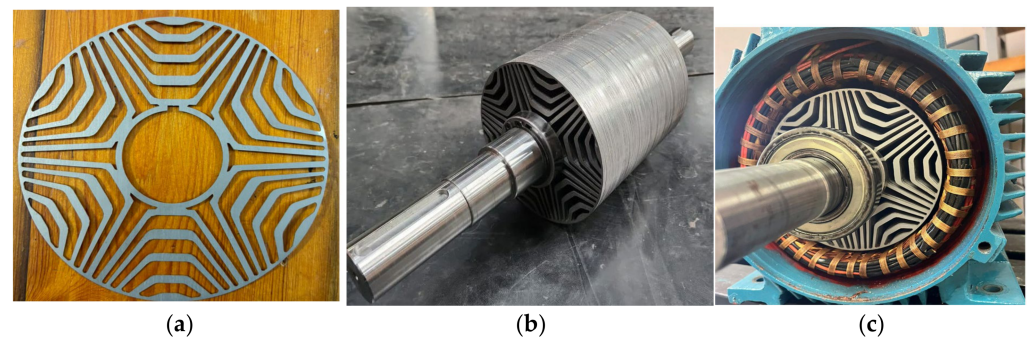
Figure 3. Photographs that show the constituents of the prototype SynRG with a slitted-rotor core. (**a**) Single rotor lamination, (**b**) Complete rotor core with shaft, (**c**) Rotor core inserted in the stator bore space ready to be fastened.

(a) (b)
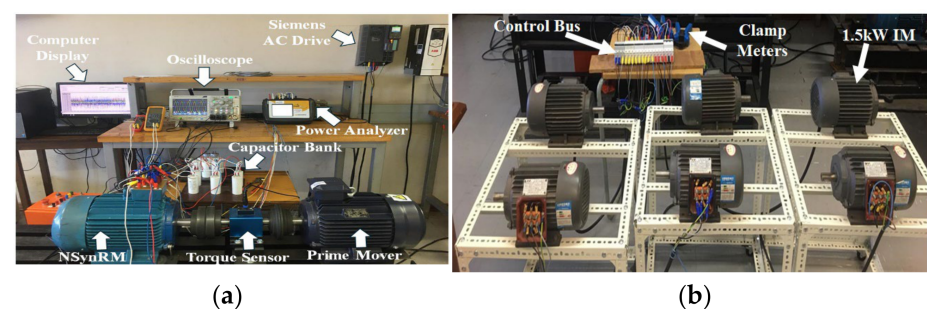
Figure 4. Photographs of the laboratory setup. (**a**) Experimental setup rig photo, (**b**) Photograph showing the inductive load scheme in the experimental setup.

A 7.5 kW induction motor controlled by a Siemens four-quadrant energy recovery AC drive is used as the prime mover to provide the required input mechanical power to the SynRG. To evaluate the ability of the proposed SynRG to feed loads with lagging power factors, a set of six induction motors were used as inductive loads as shown in Figure 4b. Under no-load conditions, the no-load induced voltage under different excitation capacitance values are evaluated. The characteristics of the no-load induced voltages are recorded in the laboratory and compared with the voltages obtained by FEA. The voltage regulation characteristics of the SynRG with a slitted-rotor core at different excitation capacitance

values for resistive, inductive, and capacitive loading obtained from the experimental test are analyzed, and the results are compared with the FEA results.

3. Finite Element Analysis Results

3.1. Analysis of Flux Density Distributions

The radial flux density distribution plots in Figure 5a–c were obtained from FEA using the AC magnetic–transient solver. The AC magnetic–transient FEA models were carried out for a loaded current of 8 A, with a constant speed of 1000 rpm. The auxiliary winding is energized with a capacitive current of 6 A. The effect of the armature reaction is noticeable in the flux density distributions shown in Figure 5. The effect of armature reaction is more magnetizing for unity and leading power factor and demagnetizing for a lagging power factor. There is heavy localized magnetic saturation on the stator back iron of SynRG when operating with leading and unity power factors. High localized magnetic saturation is also observed in some slot teeth of the SynRG when operating with leading power factors.
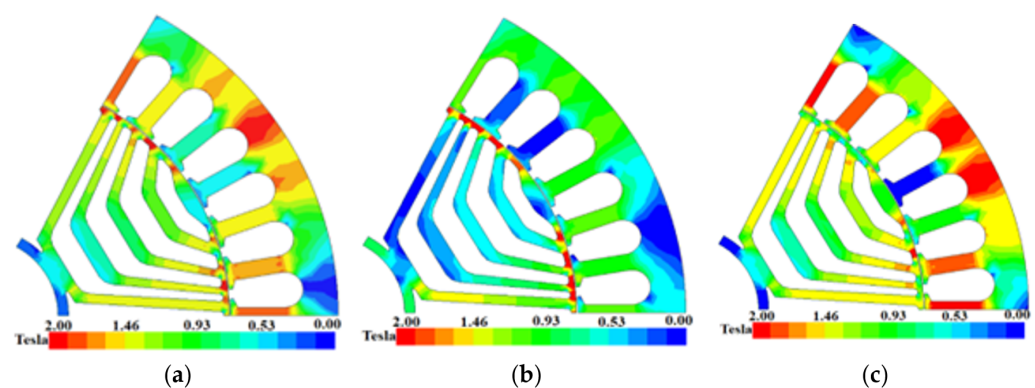

Figure 5. Flux density distribution of the SynRG with a slitted-rotor core operating with a current load of 8 A and an excitation current of 6.8 A: 1000 rpm: (**a**) Unity power factor, (**b**) Lagging power factor, (**c**) Leading power factor.

3.2. No-Load Characteristics of the SynRG

Figure 6 compares the saturation characteristics of the SynRG with a slitted-rotor core and conventional SynRG. For a constant speed of 1000 rpm, the induced no-load voltages increase with the increase in auxiliary winding excitation current. Although the SynRG with a slitted-rotor core generates more voltage with a lower excitation current, it reaches the saturation point faster than the conventional SynRG. The latter starts saturating at the excitation current of 5 A, while the SynRG with a slitted-rotor core starts saturating at the excitation current of 3.65 A. The induced no-load voltage waveforms of the SynRG with a slitted-rotor core and conventional SynRG with an excitation current of 6 A are shown in Figures 7b and 7a, respectively. The SynRGs were modeled in FEM considering the Carter factor due to stator slot opening. Its effect is quite visible in the voltage profiles shown in Figure 7. For the SynRG with a slitted-rotor core, the RMS value of the induced phase voltage is 249.3 V, which is 10.77% higher than the voltage of the conventional SynRG shown in Figure 7a. Although one may argue that the high value of the no-load induced voltage in SynRG makes it a better generator, its quick saturation may contribute to the iron loss and to the decrease in overall efficiency.
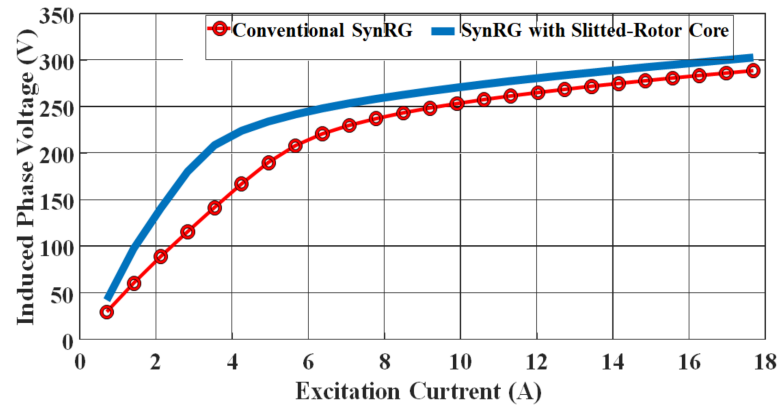
Figure 6. Comparison of saturation characteristics between the unoptimized NSynRG with a slitted-rotor core and optimized NSynRG with a slitted-rotor core.
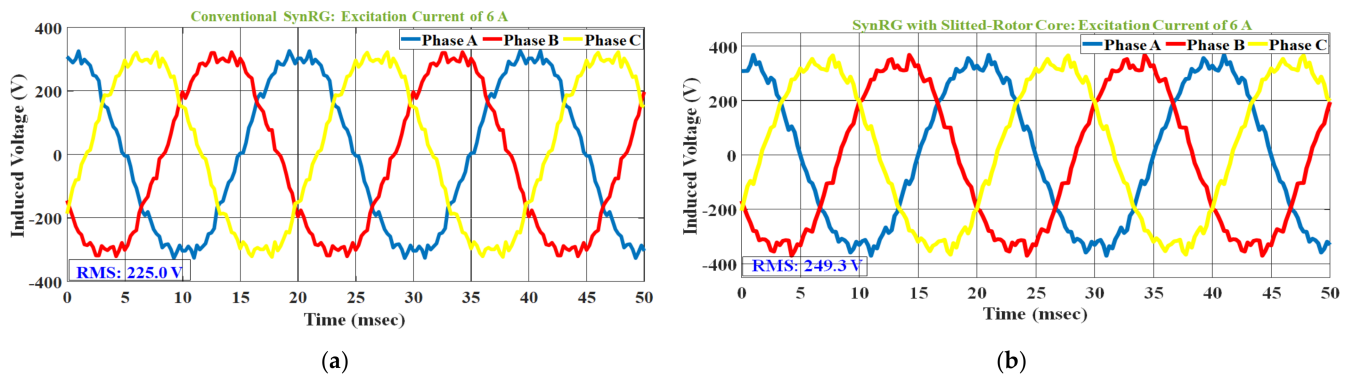

(**a**)   (**b**)

Figure 7. Induced no-load voltages with excitation current of 6 A. (**a**) Conventional SynRG, (**b**) SynRG with a slitted-rotor core.

3.3. Regulation Characteristics of the SynRG

Figure 8 depicts the regulation characteristics of the SynRGs operating at a constant speed of 1000 rpm and a constant excitation capacitive current of 6 A, supplying loads at unity, lagging, and leading power factors.
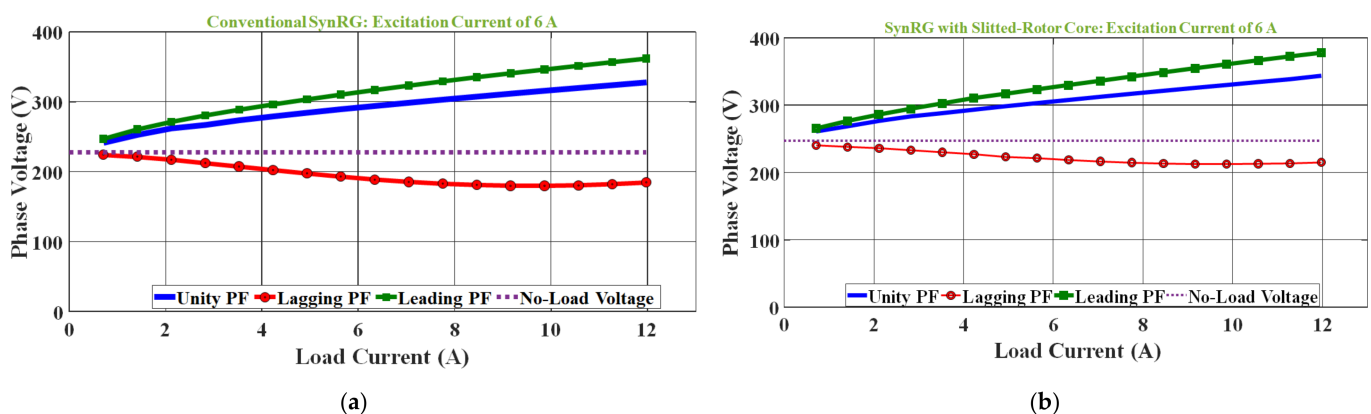

(**a**)   (**b**)

Figure 8. Airgap flux density on no-load with excitation current of 6.8 A. (**a**) The profile, (**b**) Harmonic spectrum.

It can be observed from the FEA results in Figure 8 that the voltage characteristics of the conventional SynRG and SynRG with a slitted-rotor core have the same pattern. The change of terminal voltage has an increasing characteristic when the SynRGs operate with leading and unity power factor loads and decreasing characteristics when operating

with lagging power factor loads. The percentage down voltage regulations on full load are given in Table 2. It should be noted that the voltages regulations were computed using the well-known equation as given in (1).

$$\%V_{reg} = \frac{V_o - V_{FL}}{V_o} \times 100 \tag{1}$$

where V_0 is the no-load voltage, and V_{FL} is the full-load terminal voltage. At most load currents, the percentage voltage regulations are negative for both leading and unity power factors, and they are positive for lagging power factors. Furthermore, the same results show that with a fixed excitation capacitive current of 6 A, the effect of armature reaction of the SynRG with a slitted-rotor core is demagnetizing when operating with load currents having a lagging power factor, and magnetizing when operating with load currents having unity and leading power factors.

Table 2. The percentage down voltage regulations.

Load Power Factor	Conventional SynRM	SynRG with a Slitted-Rotor Core
Unity	−37.78%	−32.37%
Lagging	20.26%	15.79%
Leading	−55.11%	−53.42%

3.4. Analysis of Electromagnetic Torque of the NSynRG

The electromagnetic torque profiles of the conventional SynRG and the SynRG with slitted-rotor core operating with an excitation current of 6.8 A when supplying a load current of 8 A with unity, leading, and lagging power factors are shown in Figure 9. The FEA results in Figure 8a,b reveal that the SynRG with a slitted-rotor core reduced the torque ripple by 24.51%, 29.72%, and 13.13% when feeding 8 A to a load with unity, lagging, and leading power factors, respectively. Another observation from Figure 8a,b shows a slight increase in the average torque for unity and lagging power factors. An interesting observation should be made when the SynRG operates with a leading power factor load. The torque developed is very small when compared to unity and lagging power factor loads. This is because the SynRG absorbs very little active power, which contributes to the development of electromagnetic torque.
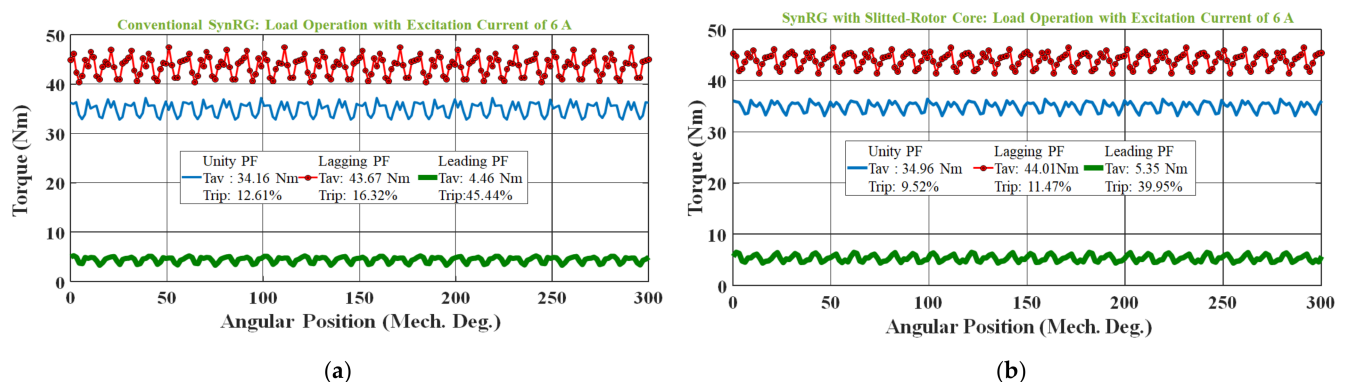

Figure 9. FEA electromagnetic torque profiles with a load current of 8 A of the NSynRG. (**a**) Unoptimized NSynRG, (**b**) Optimized NSynRG.

4. Analysis of Experimental Results

4.1. Measured No-Load Induced Voltages

The measured no-load generated voltage characteristics of the self-excited SynRG with a slitted-rotor core operating with different excitation capacitance values are shown in Figure 10. Observing the measured results in Figure 10a–c, the RMS value of the no-load voltage increases with an increase in excitation capacitance value. The increases of 3.2% and 6.7% are noted when the capacitance values are increased from 50 μF to 90 μF and 140 μF, respectively. The effect of excitation capacitance values is also noted in the harmonic components of the no-load voltage waveforms shown in Figure 10d. The 7th harmonics are dominant, and they are due to the 2nd phase-belt components of the main winding configuration. The 7th harmonics may be reduced by opting for a double-layer winding with chorded coils.
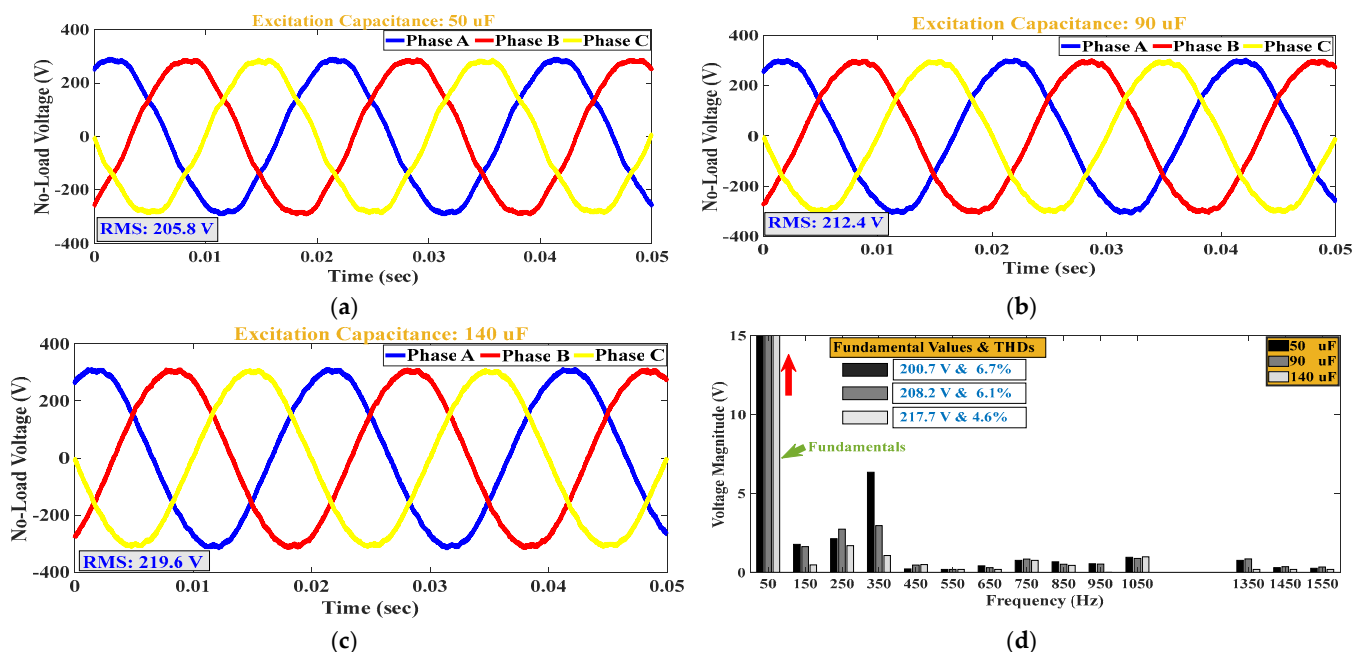

Figure 10. Generated voltage characteristics on no-load. (**a**) Excitation capacitance of 50 μF, (**b**) Excitation capacitance of 90 μF, (**c**) Excitation capacitance of 140 μF, (**d**) Harmonic components of the no-load induced voltage.

4.2. Measured Voltage Regulation Characteristics

The voltage regulation characteristics of the self-excited SynRG with a slitted-rotor core at different excitation capacitance values for resistive, inductive, and capacitive loading from the experimental measurements are shown in Figure 11.

As shown in Figure 11a–c, for any specific excitation capacitance value, the measured terminal voltages change as the load increases. Compared with the FEA results, the conventional SynRG and SynRG with slitted-rotor core measured voltage characteristics have the same pattern. The change of terminal voltage has an increasing characteristic when the SynRGs operate with capacitive and resistive loads and decreasing characteristics when operating with inductive loads. The effect of armature reaction of the SynRG with a slitted-rotor core is demagnetizing when operating with an inductive load, and magnetizing when operating with resistive and capacitive loads.
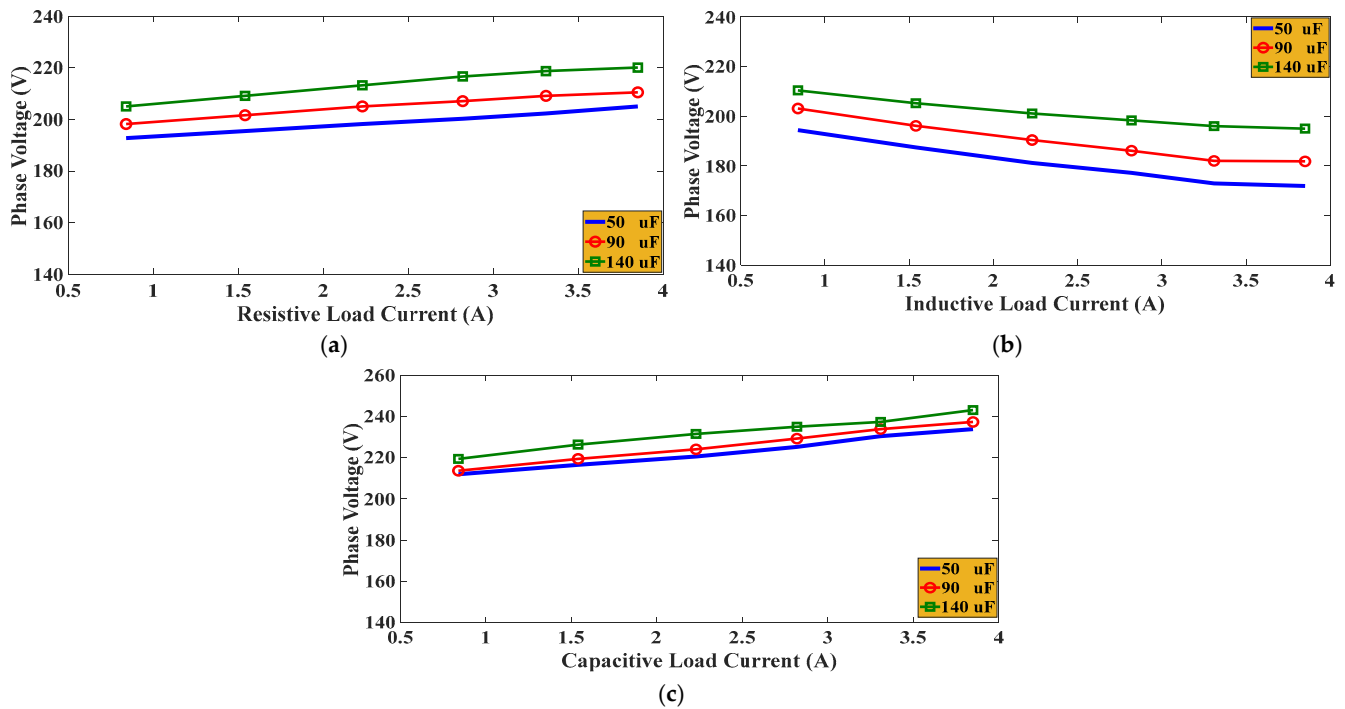
Figure 11. Regulation characteristics at different excitation capacitance values, such as (**a**) resistive load, (**b**) inductive load, and (**c**) capacitive load.

5. Dynamic Characteristics of the NSynRG

In this section, the dynamic characteristics of the SynRG with a slitted-rotor core are compared to those of the conventional SynRG in an off-grid wind power generation environment. The inertia of the rotor with slits cut in the *d*-axis is 0.000731 kgm^2, while that of the conventional rotor is 0.000877 kgm^2. The simulations were carried out using wind turbines with a rated speed of 4 m/s. The simulation has been carried out with the auxiliary stator winding connected to a 90 μF excitation capacitor. Figure 12 depicts the electromagnetic torque and speed response of the SynRG with a slitted-rotor core, while Figure 13 shows the electromagnetic torque and speed responses of the conventional SynRG. It is clearly noted in Figure 12 that the electromagnetic torque of the SynRG with a slitted-rotor core reaches its steady-state regime in just about 0.05 s after the initial oscillations, while the electromagnetic torque of the conventional SynRG in Figure 13 settles in about 0.15 s.
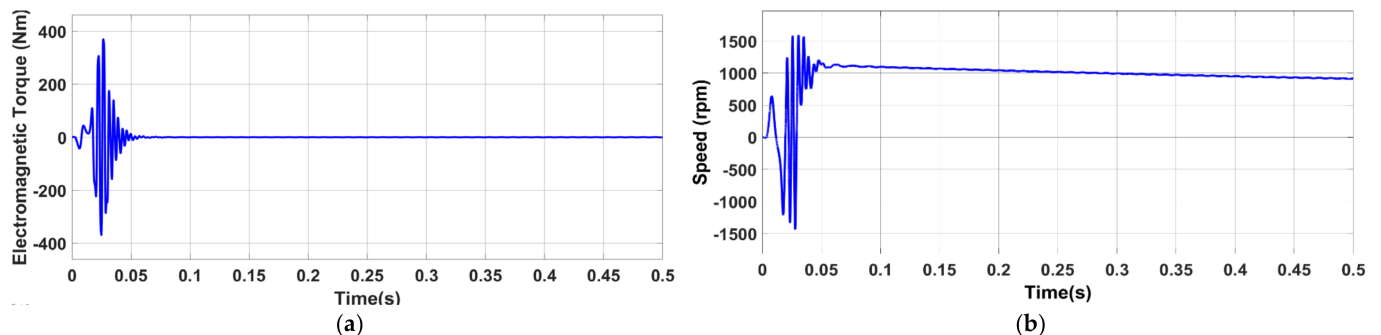

Figure 12. No-load dynamic response of the SynRG with a slitted-rotor core at a constant wind speed of 4 m/s with 90 μF excitation capacitance. (**a**) Electromagnetic Torque, (**b**) Speed.
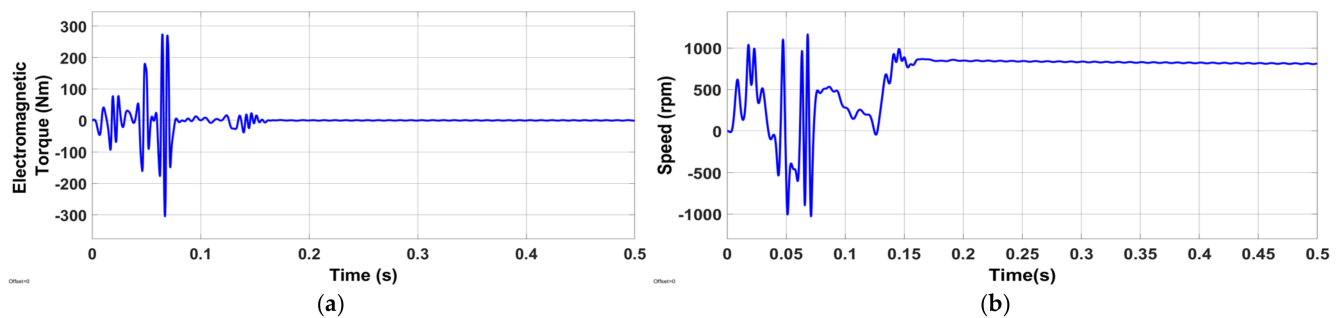
Figure 13. No-load dynamic response of the conventional SynRG rotor at a constant wind speed of 4 m/s with 90 μF excitation capacitance. (**a**) Electromagnetic Torque, (**b**) Speed.

6. Conclusions

This paper presents the performance of a dual stator winding synchronous reluctance generator with a slitted-rotor core for an off-grid wind power generation system. The FEA results reveal that the RMS value of the SynRG with a slitted-rotor core induced no-load voltage is 10% higher than that of the conventional SynRG. Furthermore, the saturation characteristics obtained from FEA show that the SynRG reaches the saturation point faster than the conventional SynRG. Additionally, there is a corroboration between FEA and experimental results as the voltage regulation characteristics exhibit the same behavior. The voltage regulations have rising characteristics when the SynRG operates with leading and unity power factor loads and falling characteristics when operating with lagging power factor loads. The effect of armature reaction of the SynRG was found to be demagnetizing when operating with an inductive load, and magnetizing when operating with resistive and capacitive loads. Another key observation in this article was the torque developed by the SynRG. The FEA results show that the SynRG with a slitted-rotor core reduced the torque ripple when operating either with load with unity, or lagging, or leading power factors, while maintaining a good average torque. Finally, the dynamic response of the SynRG with the slitted-rotor core was found to be quicker than the conventional generator, positioning it as a strong candidate in off-grid wind turbine applications. Further work on the topic presented in the paper will include analyzing the generator's performance for steady-state and transient stabilities under different load conditions and input mechanical torques.

References

1. Salameh, Z.M.; Nandu, C.V. Overview of building integrated wind energy conversion system. In Proceedings of the IEEE Power and Energy Society General Meeting, Minneapolis, MN, USA, 25–29 July 2010.
2. Goudarzi, N.; Zhu, W.D. A review on the development of wind turbine generators across the world. In Proceedings of the ASME 2012 International Mechanical Engineering Congress and Exposition, Houston, TX, USA, 9–15 November 2012.
3. Fernandez, V. Rare-earth elements market: A historical and financial perspective. *Resour. Policy* **2017**, *53*, 26–45. [CrossRef]
4. Shridhar, L. Investigations on Induction Generator for Improved Performance. Ph.D. Thesis, Department of Electrical Engineering, Indian Institute of Technology, Delhi, India, 1994.

5. Lipo, T.A. Synchronous Reluctance Machines—A Viable Alternative to AC Drives. *Electr. Mach. Power Syst.* **1991**, *19*, 659–671. [CrossRef]

6. Tefera, K.; Tripathy, P.; Adda, R. Design and Modeling of Self-Excited SRG and FM-SRG for Wind Energy Generation. In *IET Renewable Power Generation*; Wiley & Sons Ltd.: Hoboken, NJ, USA, 2021; pp. 1–17.

7. Matsuo, T.; Lipo, T.A. Rotor design optimization of synchronous reluctance machine. *IEEE Trans. Energy Convers.* **1993**, *9*, 359–363. [CrossRef]

8. Moncada, R.; Pevez, B.; Tapia, J.; Pyrhonen, J. Operation Analysis of synchronous reluctance machine in electric power generation. In Proceedings of the 2014 International Conference on Electrical Machines (ICEM), Berlin, Germany, 2–5 September 2014; pp. 2734–2739.

9. Sanada, M.; Hiramato, K.; Marinoto, S.; Takeda, Y. Torque ripple improvement for Synchronous Reluctance Motor Using Asymmetric Flux Barrier Arrangement. *IEEE Trans. Ind. Appl.* **2003**, *40*, 1076–1082. [CrossRef]

10. Fratta, A.; Troglia, G.P.; Vagati, A.; Villata, F. Evaluation of torque ripple in high performance synchronous reluctance motors. In Proceedings of the IEEE Industry Application Society Annual Meeting, Toronto, ON, Canada, 2–8 October 1993.

11. Vagati, A.; Pastorelli, M.; Franceschini, G.; Petrache, C. Design of low torque ripple synchronous reluctance motors. In Proceedings of the Annual Meeting of IEEE Conference on Industry Applications, New Orleans, LA, USA, 5–9 October 1997.

12. Xu, L.; Liu, G.; Chen, Q.; Zhao, W. Fast calculation method of optimal flux barrier-end position for torque ripple minimization in SynRMs with and without PMs. *IET Electr. Power Appl.* **2020**, *14*, 705–715. [CrossRef]

13. Bacco, G.; Bianchi, N. Choice of flux-barriers position in Synchronous Reluctance Machines. In Proceedings of the IEEE Energy Conversion Congress and Exposition (ECCE), Cincinnati, OH, USA, 1–5 October 2017; pp. 1872–1879.

14. Boldea, I. *Reluctance Synchronous Machines and Drives*; Clarendon Press: Oxford, UK, 1996.

15. Adjei-Frimpong, S.; Muteba, M. Effect of Capacitive Auxiliary Winding on a Synchronous Reluctance Motor with a Slitted-Rotor Core. In Proceedings of the 2024 4th International Conference on Electrical, Computer, Communications and Mechatronics Engineering (ICECCME), Male, Maldives, 4–6 November 2024; pp. 1–6.

16. Shimizu, K.; Yoshinari, T.; Muto, Y.; Abo, H.; Yaguchi, H. Improvement of Generating Efficiency of Vertical-axis Wind Turbine with Wind Lens. In Proceedings of the IEEE 11th Global Conference on Consumer Electronics (GCCE), Osaka, Japan, 18–21 October 2022; pp. 23–24.

17. Chandrashekhar, P.K.; Managuli, S.; Shashank, A. Design of Small-Scale Vertical Axis Wind Turbine. In Proceedings of the International Conference on Power Electronics Applications and Technology in Present Energy Scenario (PETPES), Mangalore, India, 29–31 August 2019; pp. 1–5.

18. Alger, P.; Freiburghouse, E.H.; Chase, D. Double winding for turbine alternators. *AIEE Trans.* **1930**, *49*, 226–244. [CrossRef]

19. Bassett, E.D.; Potter, E.M. Capacitive excitation for induction generators. *Electr. Eng.* **1935**, *54*, 540–545. [CrossRef]

20. Agu, L.; Anih, L.U. Enhancement of the output power of synchronous reluctance machines by capacitance injection technique. *NSE Tech. Trans* **2002**, *37*, 70–80.

21. Anih, L.U.; Obe, E.S. A new multi-stack synchronous reluctance motor. *NSE Tech. Trans.* **2004**, *39*, 53–67.

22. Ogunjuyigbe, A.; Jimoh, A.; Nicolae, D.; Obe, E. Analysis of synchronous reluctance machine with magnetically coupled three-phase windings and reactive power compensation. *IET Electric. Power Appl.* **2010**, *4*, 291–303. [CrossRef]

23. Ogunjuyigbe, A.S.O.; Jimoh, A.A.; Nicolae, D.V.; Agee, T.J. Synchronous reluctance machine with controlled capacitance injection. In Proceedings of the 2008 11th International Conference on Optimization of Electrical and Electronic Equipment, Brasov, Romania, 22–24 May 2008; pp. 39–44.

24. Ojo, O.; Dong, G.; Omoigui, M. Analysis of a Synchronous Reluctance Machine with an Auxiliary Single-Phase Winding. *IEEE Trans. Ind. Appl.* **2003**, *39*, 1307–1313.

25. Mulelu, T.K.; Muteba, M. Performance analysis of residential wind-turbine dual-stator winding synchronous reluctance generator with armature reaction effect. In Proceedings of the 8th International Conference on Renewable Energy Research and Application (ICRERA), Brasov, Romania, 3–6 November 2019.